Optics Letters

Photonics-based dual-functional system for simultaneous high-resolution radar imaging and fast frequency measurement

Jingzhan Shi,[1] Fangzheng Zhang,[1,2] Xingwei Ye,[1] Yue Yang,[1] De Ben,[1] and Shilong Pan[1,3]

[1]Key Laboratory of Radar Imaging and Microwave Photonics, Ministry of Education, Nanjing University of Aeronautics and Astronautics, Nanjing 210016, China
[2]e-mail: zhangfangzheng@nuaa.edu.cn
[3]e-mail: pans@nuaa.edu.cn

Received 27 December 2018; revised 14 March 2019; accepted 15 March 2019; posted 15 March 2019 (Doc. ID 356410); published 5 April 2019

A photonics-based dual-functional system is proposed that can simultaneously implement high-resolution radar imaging and fast frequency measurement. In this system, the radar is realized based on photonic frequency doubling and de-chirp receiving, and the frequency measurement is achieved by a novel frequency-to-time mapping method. In the experimental demonstration, the radar works in Ku band with a bandwidth of 6 GHz (12–18 GHz), through which inverse synthetic aperture radar imaging with a resolution as high as ∼2.6 cm × ∼2.8 cm is achieved. The frequency measurement module operates in Ka band, which can achieve a measurement frequency range from 28 GHz to 37 GHz, with a measurement resolution of 40 MHz and a refresh rate of 100 kHz.

https://doi.org/10.1364/OL.44.001948

Radar, electronic warfare (EW), and communications are indispensable functions in military applications. In order to reduce the cost and volume of hardware, incorporating multiple functions within an integrated system is required. For example, the Office of Naval Research initiated a program to demonstrate the integration of several shipboard RF functions (radar, EW, and communications) utilizing a common set of broadband apertures, signal and data processing, signal generation, and display hardware [1].

Microwave photonics (MWPs) has the advantages of high frequency, large bandwidth, low transmission loss, and resistance to electromagnetic interference [2]. In recent years, more and more investigations on MWPs have been conducted to overcome the bandwidth limitations in radar and EW systems. Up to now, several photonics-based radar architectures have been proposed [3–6]. The potential bandwidth of the photonics-based radar can reach tens of gigahertz, enabling ultra-high-resolution detection and imaging. As for EW systems, an important application of MWPs is wide-range frequency measurement, which can be implemented by frequency-to-power mapping, frequency-to-time mapping, and frequency-to-space mapping techniques [7–11]. However, in previous demonstrations, the photonics-based radar detection function and the frequency measurement function are usually implemented by independent systems.

In this Letter, we propose a photonics-based dual-functional system that can simultaneously implement high-resolution radar imaging and fast frequency measurement. In this system, the radar is realized based on photonic frequency doubling and de-chirp receiving, and the frequency measurement is implemented by a novel frequency-to-time mapping method. Figure 1 shows the schematic diagram of the proposed system. A laser diode (LD) is used as the continuous wave (CW) light source. It is modulated by a dual-polarization Mach–Zehnder modulator (Dpol-MZM) to generate a polarization-multiplexed optical signal [12]. In x polarization (X-pol), the sub-MZM is driven by an intermediate frequency band linear frequency modulation (IF-LFM) signal generated by an arbitrary waveform generator (AWG). In y polarization (Y-pol), the sub-MZM is driven by the signal under test (SUT), which is collected by the frequency measurement receiver antenna and passed through an electrical bandpass filter (EBPF). The two sub-MZMs are both biased at the minimum transmission point to suppress the even-order modulation sidebands. The instantaneous optical spectrum of the obtained polarization multiplexed signal at point a is illustrated in Fig. 1, where f_c, f_L, and f_x are the frequency of the optical carrier, IF-LFM signal, and SUT, respectively. For ease of understanding, the instantaneous frequency of the IF-LFM signal in a single period is assumed to be $f_L(t) = f_0 + kt(0 < t \le T)$, in which f_0 is the initial frequency, k is the chirp rate, and T is the temporal period. The obtained polarization-multiplexed signal is amplified by an erbium-doped fiber amplifier (EDFA). Then, the signals in X-pol and Y-pol are separated by a polarization beam splitter (PBS). In the upper branch, the optical signal in X-pol (point b) is sent to a reconfigurable optical BPF (ROBPF), which has two output ports. In one output port of the ROBPF, the ±1st-order frequency-sweeping sidebands are filtered out (the spectrum at point c) and used for radar applications. In the other output port of the ROBPF, one of the third-order sidebands is selected (the spectrum at point d), and used as

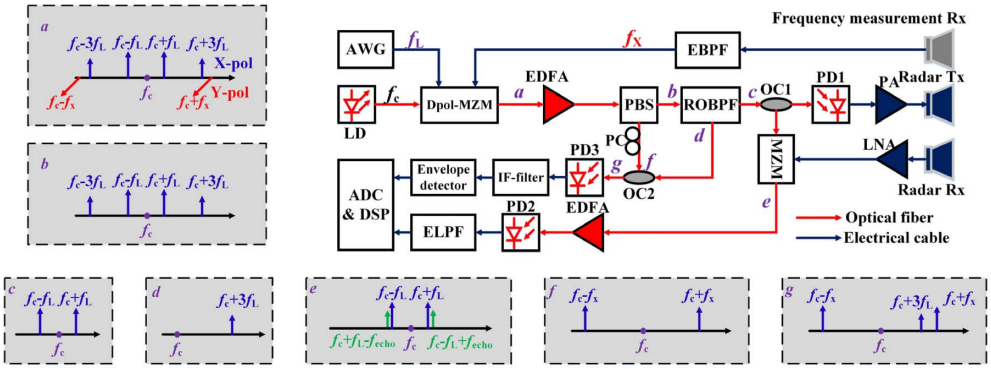

Fig. 1. Schematic diagram of the photonics-based dual-functional system. LD, laser diode; AWG, arbitrary waveform generator; MZM, Mach–Zehnder modulator; Dpol-MZM, dual-polarization MZM; DEFA, erbium-doped fiber amplifier; PBS, polarization beam splitter; ROBPF, reconfigurable optical bandpass filter; OC, optical coupler; PD, photodetector; PA, power amplifier; LNA, low-noise amplifier; EBPF, electrical bandpass filter; ELPF, electrical lowpass filter; ADC, analog-to-digital converter; DSP, digital signal processor.

the frequency-sweeping reference to implement frequency measurement.

To implement radar detection and imaging, the optical signal at point *c* is split into two branches by an optical coupler (OC1). The signal in one branch is sent to a photodetector (PD1) to generate an LFM signal, of which the center frequency and bandwidth are doubled compared with the IF-LFM signal. The obtained LFM signal is amplified by a power amplifier (PA) before being launched to the air by a transmit antenna. The radar echo with an instantaneous frequency of f_{echo} is collected by the receiving antenna and amplified by a low-noise amplifier (LNA). The amplified signal is used to drive an MZM to modulate the optical signal from the other output port of OC1. After the MZM (point *e*), a frequency pair at $f_c - f_L$ and $f_c + f_L - f_{\text{echo}}$, and another frequency pair at $f_c + f_L$ and $f_c - f_L + f_{\text{echo}}$, are generated because of the electro-optical modulation by the MZM. This optical signal is properly amplified by an EDFA and sent to a PD (PD2) to implement photonic-mixing-based de-chirping of the radar echoes [4]. Next, an electrical lowpass filter (ELPF) is used to select the de-chirped signal, which is then digitized by an analog-to-digital converter (ADC) and processed by the digital signal processing (DSP) unit.

To measure the frequency of the SUT, the optical frequency-sweeping reference signal at point *d* is combined with the optical signal in Y-pol from the PBS, by another optical coupler (OC2). Before the two signals are combined, the polarization of the signal from the PBS is adjusted by a polarization controller (PC) to be aligned with that of the frequency-sweeping reference signal, as shown by the spectrum at point *f*. The combined optical signal (point *g*) is sent to another PD (PD3) to perform photonic frequency down-conversion. After PD3, a narrow band IF filter with a center frequency of f_{IF} is applied to select the frequency component at f_{IF}. An envelope detector is followed to detect the pulse envelope, of which the instantaneous amplitude is proportional to the power of the frequency component at $f_{\text{IF}} + 3f_{\text{L}}$ of the SUT, i.e.,

$$A(t) = \alpha S(f_{\text{IF}} + 3f_{\text{L}}) = \alpha S(f_{\text{IF}} + 3f_0 + 3kt), \quad \textbf{(1)}$$

where $A(t)$ is the signal after the envelope detector, $S(x)$ is the spectral amplitude of the SUT at frequency x, and α is a coefficient determined by the amplitude of the optical frequency-sweeping reference and the responsibility of PD. In obtaining (1), only the frequency mixing between $f_c + 3f_L$ and $f_c + f_x$ is considered. When f_x is in the frequency range of $f_{\text{IF}} + 3f_0$ to $f_{\text{IF}} + 3f_0 + 3kT$, which can be constrained by choosing a proper bandwidth of the EBPF after the receive antenna, its spectrum amplitude can be obtained based on (1). In this process, the spectral information of the SUT is mapped to the time domain, i.e., microwave frequency-to-time mapping is implemented. When the temporal signal is sampled by an ADC, the frequency of the SUT can be estimated according to the time position corresponding to a certain frequency component. Here, the use of a third-order sideband helps to achieve a frequency measurement range three times the sweeping bandwidth of the IF-LFM signal. If a higher-order sideband is adopted, the frequency measurement range can be further enlarged. To avoid spectral aliasing between adjacent sidebands, the highest sideband that can be used for frequency measurement should have an order less than $2f_0/kT$. Also, the frequency measurement range and speed can be easily controlled by tuning the bandwidth and duration of the IF-LFM signal. In addition to these advantages, photonics-based frequency mixing features a larger operation bandwidth over 10 GHz [13].

A proof-of-concept experiment is carried out. The IF-LFM signal generated by the AWG has a bandwidth of 3 GHz (6–9 GHz) and a repetition rate of 100 kHz, and a passband filter centered at 10 GHz with a 3-dB bandwidth of 15 MHz is used as the IF filter. The spectra of the modulated signal injected into the ROBPF and the signals after the ROBPF, and the response of the ROBPF are measured by an optical spectrum analyzer (YOKOGAWA, AQ6370C) with the results shown in Fig. 2. First, the radar function is investigated based on the established system. In this investigation, the de-chirped signals after the ELPF are sampled by a real-time oscilloscope working at a sampling rate of 50 MSa/s, which limits the maximum detection range of the radar to be about 6.25 m. For practical EW applications, the detection range should be further improved by increasing the sampling rate and/or decreasing the chirp rate of the IF-LFM signal. The waveform of the transmitted LFM signal in one period (10 μs) at the output of the PA is observed by an 80-GSa/s oscilloscope (Keysight, DSO-X 92504A), as plotted in Fig. 3(a). Figure 3(b) shows the corresponding instantaneous frequency of the LFM signal.

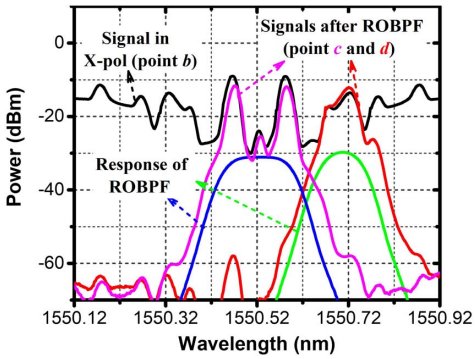

Fig. 2. Spectra of the signal injected into the ROBPF and the signals after the ROBPF, and the response of the ROBPF.

It can be seen that the LFM signal has a bandwidth of 6 GHz (12–18 GHz), indicating successful frequency doubling is achieved. To investigate the radar detection performance, two rectangular sheet metals (size: 4.5 cm × 6.5 cm) are used as the targets. When the two targets are located 126.0 cm and 144.0 cm away from the antenna pair, respectively, the power spectrum of the de-chirped signal is calculated and shown in Fig. 4(a). In Fig. 4(a), the two spectral peaks at 5.030 MHz and 5.765 MHz correspond to the two targets. To check the range resolution of the radar, one of the peaks in Fig. 4(a) is zoomed in, as shown in Fig. 4(b). It can be seen that the 3-dB bandwidth of the peak is 0.105 MHz, indicating a range resolution as high as 2.6 cm is achieved. Then, high-resolution inverse synthetic aperture radar (ISAR) imaging is demonstrated. As shown in Fig. 5(a), the target is placed on a turntable that rotates with a speed of 360 deg per second. The target is a capital letter "A" composed of several small trihedral corner reflectors (size: 2 cm × 2 cm × 2 cm), and the distance between two adjacent reflectors is about 4.5 cm, as shown in Fig. 5(b). The ISAR image is constructed based on two-dimensional Fourier transformation using the de-chirped signal in a temporal period of 0.056 s. Figure 5(c) shows the obtained ISAR image. According to the parameters above and the formula provided by [6], the cross-range resolution of the obtained ISAR image is about 2.8 cm, which indicates the ability to separate two closely spaced scatterer centers along the cross-range direction.

For frequency measurement, considering the IF frequency is 10 GHz and the tripled frequency of the IF-LFM signal is from 18 GHz to 27 GHz, the frequency measurement range is from 28 GHz to 37 GHz. The time for a single measurement is determined mainly by the time required for the frequency-sweep

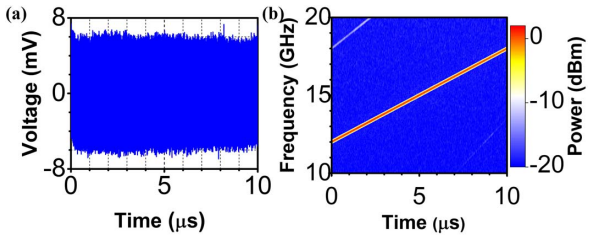

Fig. 3. (a) Waveform and (b) corresponding instantaneous frequency of the transmitted LFM signal in one period (10 μs).

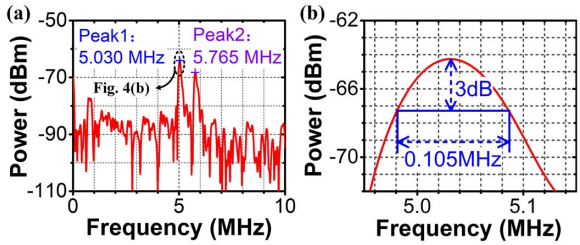

Fig. 4. (a) Power spectrum of de-chirped signal when the two targets are separated by approximately 18 cm, and (b) 3-dB bandwidth of the power spectrum of de-chirped signal.

LFM signal to complete a single scan; thus, the time for a single measurement in this experiment is 10 μs. To further improve measurement speed, an IF-LFM signal with a higher repetition rate can be adopted. To test frequency measurement performance, a single-frequency signal at 33 GHz generated by a signal generator (Agilent, E8257D) is used as the SUT. Figure 6 shows the waveform acquired by the ADC in a period of 10 μs, where a short pulse appears at the time position of 5.54 μs. According to the frequency-to-time mapping principle, the estimated frequency corresponding to this time position is 32.986 GHz, and the frequency measurement error is −14 MHz. Based on (1), the spectral amplitude can also be derived, once the coefficient α is figured out by a simple calibration using a signal with known spectral amplitude. Figure 7(a) shows the measured frequency-to-time mapping relationship when the frequency of the SUT changes from 28 GHz to 37 GHz with a step of 1 GHz, which agrees well with the theoretical result. Figure 7(b) shows the measurement error as a function of the input frequency. It can be seen that the errors are kept within ±15 MHz in the whole operating bandwidth. When a two-tone microwave signal at 30 GHz

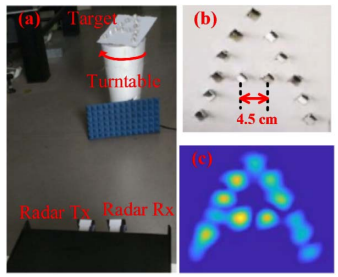

Fig. 5. (a) Target, (b) experimental scene, and (c) obtained ISAR image for the demonstration of radar imaging.

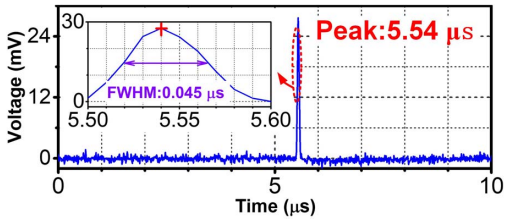

Fig. 6. Waveform acquired by the ADC when a single-frequency signal with a frequency of 33 GHz is under test.

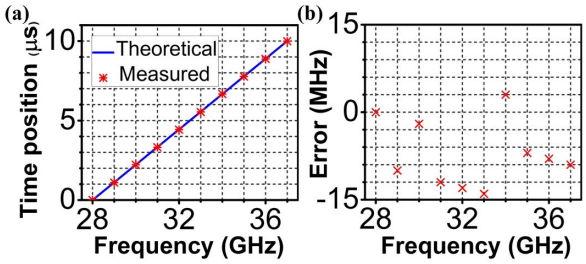

Fig. 7. (a) Measured and theoretical time position of the pulse, and (b) measurement errors versus the input frequencies.

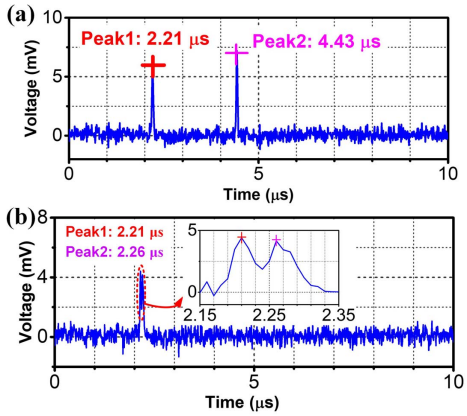

Fig. 8. Waveform acquired by the ADC when a two-tone signal has a frequency spacing of (a) 2 GHz and (b) 40 MHz is under test, respectively.

and 32 GHz is used as the SUT, the signal acquired by the ADC is shown in Fig. 8(a), where two short pulses at time positions of 2.21 μs and 4.43 μs are observed, indicating the proposed system can also measure the signals with multiple frequencies.

The frequency measurement resolution is also investigated. When measuring a single-frequency signal, the full width at half maximum (FWHM) of the short pulse is about 0.045 μs, as shown in the inset in Fig. 6. This value is determined by the rise-and-fall time $(2 * 0.35/B_{\mathrm{IF}})$ of the IF filter, where B_{IF} is the 3-dB bandwidth of the IF filter [14]. Based on the frequency-to-time-mapping relationship, the duration of 0.045 μs corresponds to a frequency spacing of 40 MHz, which means the frequency measurement resolution is 40 MHz. In the experiment, when a two-tone signal with a 40-MHz frequency spacing (at 30 GHz and 30.04 GHz) is used as the SUT, the two pulses in the signal acquired by the ADC can still be distinguished, as shown in Fig. 8(b). This result shows that a measurement resolution of 40 MHz is achieved, which is much better than those achieved by other frequency-to-time mapping methods [9,10].

Finally, the fundamental and the third-order intermodulation distortion (IMD3) levels are measured when the power of

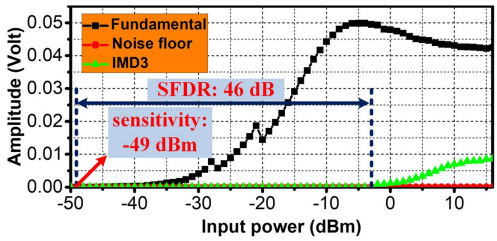

Fig. 9. Fundamental and IMD3 levels versus the input RF power.

the SUT increases from −50 dBm to 16 dBm. This is achieved by analyzing the time domain signal after frequency-to-time mapping of a two-tone signal with a frequency spacing of 100 MHz, and the result is shown in Fig. 9. As can be seen, the sensitivity of the frequency measurement receiver is −49 dBm, and the spurious free dynamic range (SFDR) is 46 dB.

In conclusion, we have proposed and demonstrated a photonics-based dual-functional system for simultaneous radar imaging and frequency measurement. The experiment results show the advantages of the proposed system, which is a possible solution to future electric systems with multiple functions.

Funding. National Natural Science Foundation of China (NSFC) (61871214); Natural Science Foundation of Jiangsu Province (BK20180066); The Jiangsu Provincial Program for High-level Talents in Six Areas (DZXX-005); Fundamental Research Funds for the Central Universities (NS2018028); Postgraduate Research & Practice Innovation Program of Jiangsu Province (KYCX17_0289).

REFERENCES

1. P. Hughes and I. Choe, in *Proceedings IEEE International Conference on Phased Array Systems and Technology* (2000), pp. 21.
2. J. Yao, J. Lightwave Technol. **27**, 314 (2009).
3. P. Ghelfi, F. Laghezza, F. Scotti, G. Serafino, A. Capria, S. Pinna, D. Onori, C. Porzi, M. Scaffardi, A. Malacarne, V. Vercesi, E. Lazzeri, F. Berizzi, and A. Bogoni, Nature **507**, 341 (2014).
4. F. Zhang, Q. Guo, and S. Pan, Sci. Rep. **7**, 13848 (2017).
5. S. Peng, S. Li, X. Xue, X. Xiao, D. Wu, X. Zheng, and B. Zhou, Opt. Express **26**, 1978 (2018).
6. F. Zhang, Q. Guo, Z. Wang, P. Zhou, G. Zhang, J. Sun, and S. Pan, Opt. Express **25**, 16274 (2017).
7. S. Pan and J. Yao, J. Lightwave Technol. **35**, 3498 (2016).
8. X. Zou, B. Lu, W. Pan, L. Yan, A. Stöhr, and J. Yao, Laser Photon. Rev. **10**, 711 (2016).
9. L. Nguyen, IEEE Photon. Technol. Lett. **21**, 642 (2009).
10. T. A. Nguyen, E. H. W. Chan, and R. A. Minasian, Opt. Lett. **39**, 2419 (2014).
11. W. Wang, R. Davis, T. Jung, R. Lodenkamper, L. Lembo, J. Brock, and M. Wu, IEEE Trans. Microw. Theory Tech. **49**, 1996 (2001).
12. F. Zhang, B. Gao, P. Zhou, and S. Pan, IEEE Photon. Technol. Lett. **28**, 1645 (2016).
13. G. Gopalakrishnan, W. Burns, and C. Bulmer, IEEE Trans. Microw. Theory Tech. **41**, 2383 (1993).
14. C. Mittermayer and A. Steininger, IEEE Trans. Instrum. Meas. **48**, 1103 (1999).